Soil & Tillage Research 258 (2026) 107005

Contents lists available at ScienceDirect

Soil & Tillage Research

journal homepage: www.elsevier.com/locate/still

Thickness variation of black soil on sloping farmland in northeast China from 1963 to 2023

Chang Liu [a], Gang Liu [a,b,*], Chenxi Dan [a], Enshuai Shen [a], Ya Liu [a], Qiong Zhang [a], Han Luo [a], Chutian Zhang [a], Zhen Guo [c], Kaishan Song [d]

[a] *State Key Laboratory of Soil and Water Conservation and Desertification Control, College of Soil and Water Conservation Science and Engineering (Institute of Soil and Water Conservation), Northwest A&F University, Yangling 712100, China*
[b] *Institute of Soil and Water Conservation of Chinese Academy of Sciences and Ministry of Water Resources, Yangling 712100, China*
[c] *Sichuan Huabiaoce Testing Technology Co. Ltd., Chengdu 610097, China*
[d] *The Northeast Institute of Geography and Agricultural Ecology, Chinese Academy of Sciences, Jilin 130102, China*

A R T I C L E I N F O

Keywords:
Slope shapes
Black soil thickness
Evolutionary process
Distribution characteristics
Restore simulation

A B S T R A C T

The black soil thickness (BST) serves as a critical indicator for assessing soil quality in northeast China. Nevertheless, the spatial distribution and variability of BST in sloping farmland remain inadequately understood. Especially, after many years of cultivation and erosion, this spatial variability increased. The aim of this research is to examine the variations in the BST on sloping farmland over the past semi-century. Three slopes in 150–200 m length with shapes of straight, convex, and concave in Bin County, Heilongjiang Province, were selected. The ^{137}Cs nuclide tracing technology and ground-penetrating radar technology were utilized to analyze the distribution characteristics of soil erosion-deposition and BST on the three slopes, respectively. Furthermore, the distribution characteristics of BST on the three slopes over the past semi-century were reconstructed by using the historical soil erosion-deposition rates. The findings revealed that the soil erosion rate, arranged in descending order, are as follows: concave slope, convex slope, straight slope. The average BST in 2023 is as follows: convex slope > straight slope > concave slope, whereas in 1963 is as follows: concave slope > convex slope > straight slope. The reconstructed BST indicates notable variations in thickness across different shapes of slopes. In the past semi-century, the average soil erosion rate on three slopes were 0.17 cm a^{-1}. However, the processes of erosion and deposition occurring on concave and convex slopes resulted solely in alterations to the local slope gradient, without influencing the overall classification of the slope type. Consequently, this study provided a precise depiction of the spatial variation characteristics and thinning rate of the black soil in past years, that can furnish a scientific foundation for forecasting soil erosion and safeguarding black soil resources.

1. Introduction

Soil is a fundamental global resource and a critical component of natural ecosystems, with its thickness directly influencing productivity and hydrological functions (Meyer et al., 2007; Duan et al., 2011). The black soil region in northeast China, is one of the four major black soil distribution areas in the world (Sorokin et al., 2020), and serves as a critical foundation for grain production in China. Heilongjiang Province is located in the central zone of the black soil region, where occupied 56.1 % of the total farmland in the typical black soil region of northeast China (General Office of the People's Government of Heilongjiang Province, 2021). The most of soil in this region has been used for agricultural production over 50 years (Liu et al., 2012). Nevertheless, due to the lack of effective soil conservation strategies and the adoption of unsustainable agricultural techniques, there has been a marked decline in soil quality. This deterioration poses a significant threat to both national food security and ecological integrity (Ministry of Agriculture and Rural Affairs of the People's Republic of China, 2017).

Soil erosion represents a significant factor contributing to soil degradation in cultivated land. The application of ^{137}Cs technology presents distinct benefits for investigating soil erosion-deposition processes. ^{137}Cs is an artificial radionuclide (with a half-life of approximately 30.17 years), which is a byproduct generated from atmospheric nuclear tests and nuclear leaks since the 20th century (Hedvall et al.,

* Correspondence to: Institute of Soil and Water Conservation, Northwest A&F University, No. 26, Xinong Road, Yangling, Shaanxi Province 712100, China.
E-mail addresses: gliu@foxmail.com, gangliu@nwafu.edu.cn (G. Liu).

https://doi.org/10.1016/j.still.2025.107005
Received 28 July 2025; Received in revised form 2 December 2025; Accepted 4 December 2025
Available online 6 December 2025
0167-1987/

1996). After depositing on the ground surface, ^{137}Cs is strongly adsorbed by clay particles in the soil, making it difficult to be leached downward by water, and thus only migrates with soil particles (Zhang et al., 1990). Therefore, it is regarded as a good tracer and has been widely used in studies on the multi-year average soil erosion rate. Fang et al. (2012) employed ^{137}Cs tracing technology to assess the spatial distribution of soil redistribution within the Heshan Farm watershed located in Heilongjiang Province. Yang et al. (2011) conducted a quantitative assessment of soil erosion rates at field and small watershed scales by using ^{137}Cs and ^{210}Pb$_{ex}$ techniques, and indicated that the BST will be completely eroded within 70 years. Nevertheless, erosion-deposition processes directly affect the dynamic changes in BST (Liu et al., 2023). Topography serves as a key factor in soil erosion processes, with its influence primarily manifested through slope gradient, slope length, and slope shape. Slope shape, essentially a spatial combination of gradient and length, jointly affects erosion through their synergistic interaction (Xie et al., 2023). Specifically, slope shape significantly alters micro-topographic characteristics, thereby modifying convergence pathways and flow velocity distribution of surface runoff. Studies have shown that erosion patterns along slopes are strongly influenced by slope shape: convex slopes exhibit the most severe erosion at the back of slope, whereas concave slopes experience peak erosion at the shoulder of slope (An et al., 2014). Furthermore, natural soil-forming processes constitute the foundation for black soil formation. Weathering products of parent rock provide the material basis, while vegetation anchors soil through root systems and accumulates organic matter, thereby promoting the gradual thickening of the black soil layer.

The variations in the BST serve as crucial indicators for evaluating the black soil degradation (Duan et al., 2011). Conventional soil thickness measurement techniques, such as soil drilling and profile methods (Emmet-Booth et al., 2019; Morse et al., 2012), exhibit significant limitations. Utilizing the profile method as a case study, it is common in practical field operations to select a restricted number of points for profile excavation across an extensive area. By systematically observing and measuring these profiles, one can extrapolate the BST throughout the entire region. However, due to the discontinuity of sampling points, it is impossible to comprehensively and accurately reflect areas with abrupt changes in thickness. In contrast, the determination of BST utilizing ground penetrating radar (GPR) technology demonstrates a degree of continuity and enhanced accuracy (Liu et al., 2021). GPR technology is a method that uses high-frequency electromagnetic pulse wave reflections (Morey, 1974). It detects the distribution patterns and characteristics of underground targets (Persico, 2014). Additionally, it can continuously detect soil stratigraphic structures. Currently, the characterization of black soil thickness varies considerably across studies. Zhang et al. (2007) undertook a comprehensive investigation of the northeast black soil region, revealing that the average BST in 1982 was measured at 43.7 cm. By the year 2002, it was observed that the proportion of land exhibiting a BST of less than 30 cm constituted 40.9 % of the overall area. Furthermore, Yang et al. (2003) reported that in certain regions of northeast China, the mollic horizon has completely disappeared. The variability in the distribution of BST presents significant challenges to conventional techniques employed for measuring this parameter. Liu et al. (2022) conducted field drilling and profile measurements across 61 profiles from the second soil survey, revealing that the average thickness of the black soil in Heilongjiang Province has diminished by 6.83 cm over the course of nearly four decades. Furthermore, Yang et al. (2011) estimated the soil erosion rate on slopes in Jilin Province to be 1.99 mm a^{-1}, noting considerable variability across distinct slope positions. Concurrently, the integration of GPR with the ^{137}Cs tracing technology enables us to make initial assessments regarding the alterations in the thickness of the black soil over the past semi-century, while also facilitating a more precise quantification of the erosion thickness of soil layer. Therefore, a systematic investigation of the spatial configuration of BST and quantification of black soil thinning rates are critically required.

The main objectives of this study were: (i) to investigate the spatial distribution characteristics of soil erosion-deposition rates on slopes with different shapes; (ii) to explore the characteristics of changes in the BST on different slopes from 1963 to 2023; (iii) to analyze the evolutionary process of the black soil on different slopes. This study establishes a scientific foundation for black soil conservation and provides data essential for strategic soil and water conservation measures.

2. Materials and methods

2.1. Study areas

The study site is located in Bin County, which is part of Harbin City in Heilongjiang Province, in northeast China (45°45′40″-45°52′19″N, 127°24′24″-127°28′56″E) (Fig. 1). This area belongs to a temperate continental monsoon climate, which is characterized by cold and dry winters and hot summers with significant precipitation. The mean annual temperature is 3.9°C, with an annual accumulated temperature of 3200°C. Furthermore, the average annual rainfall was 550 mm, with approximately 80 % of this rainfall concentrated between the months of May and September (Feng et al., 2018). The predominant topographical feature of the region consists of rolling hills. The soil texture in the study area is classified as silty clay loam. In this investigation, the black soil is categorized as Hapli–Udic Isohumosols under the Chinese Soil Taxonomy (CST), classified as Mollisols (Agriboroll subgroup) within the USDA Soil Taxonomy, and designated as Haplic Phaeozems in the FAO-UNESCO soil classification system (National Soil Survey Office, 1998; Gao et al., 2015; Feng et al., 2018). The typical soil profile is characterized by a distinct A-B-C horizon sequence. Specifically, the uppermost A horizon (surface layer), also termed the topsoil or mollic epipedon, is distinguished by its elevated organic matter content, which confers a darker coloration compared to the underlying horizons. In this study, the A horizon is defined as the black soil thickness (BST). The B horizon (subsoil) typically accumulates clay minerals and iron oxides leached from the overlying A horizon, resulting in a diagnostic dark gray to brownish hue. The C horizon, as the parent material, comprises primary geological deposits such as Quaternary lacustrine/fluvial sand beds or loess sediments, serving as the foundational material from which the overlying soil horizons develop (Gao et al., 2015).

Within the study site, three distinct sloping farmlands were identified, each exhibiting unique slope characteristics (Table 1). The straight slope was 200 m in length and 130 m in width, with an average slope gradient of 1.91°. The convex slope was 168 m in length and 70 m in width, with an average slope gradient of 2.48°. The concave slope was 150 m in length and 60 m in width, with an average slope gradient of 3.19°. Their geographically proximate locations ensured consistent regional climate, agricultural policies, and technical extension backgrounds over recent decades. Field investigations and interviews with farmers indicated that the three slopes exhibit consistent historical management practices. Specifically, they have traditionally employed contour plowing and maintained a corn-soybean crop rotation system, with no major land use changes or special local soil and water conservation projects. Notably, all slope surfaces are natural terrains of the north-facing slope, preserving original topographic features without artificial modification.

2.2. Soil sample collection

This research involved the collection of two distinct sets of soil samples, all of which were obtained along the GPR survey lines. One set of samples was designated for the assessment of fundamental soil characteristics, including bulk density, soil texture, and organic matter content. The second set was utilized for the analysis of ^{137}Cs activity. In October 2023, soil samples for the assessment of fundamental soil properties were obtained using a soil auger at three distinct slope positions: the top, middle slope, and toe of the slope. At each slope

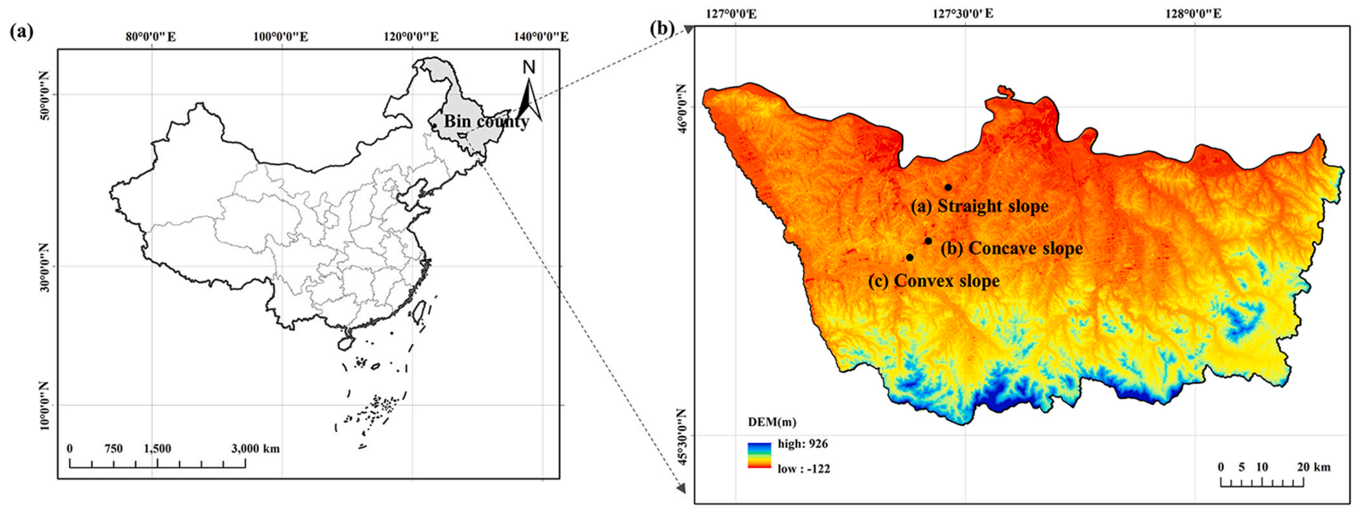

Fig. 1. Schematic diagram illustrating the distribution of three distinct slope shapes in Bin County of Heilongjiang Province, China. The county map is based on the standard map released by the Ministry of Natural Resources of the People's Republic of China [No. GS(2019)1822].

Table 1
The topographic and soil properties on three study slopes in Bin County of Heilongjiang Province, China.

	Straight slope	Convex slope	Concave slope
Slope length (m)	200	168	150
Slope width (m)	132	70	60
Slope gradient (°)	1.91	2.48	3.19
Clay %	33.89 ± 2.84	30.66 ± 1.54	28.85 ± 2.66
Silt %	59.13 ± 1.84	60.00 ± 0.46	59.47 ± 1.97
Sand %	6.98 ± 1.02	9.34 ± 1.91	11.68 ± 1.04
Bulk density (g cm^{-3})	1.47 ± 0.17	1.56 ± 0.16	1.51 ± 0.59
Soil moisture (%)	24.01 ± 0.76	22.65 ± 0.52	23.94 ± 1.75
Organic matter (g kg^{-1})	26.84 ± 2.25	21.39 ± 4.32	25.59 ± 5.78

position, three replicate sampling locations were established, with samples collected to a depth of 30 cm. Bulk density was determined using a volumetric ring sampler at a consistent sampling depth of 30 cm. Soil samples were obtained in stratified layers corresponding to depths of 0–10 cm, 10–20 cm, and 20–30 cm, with one sample collected from each respective layer. Three replicates were also set for each slope position. Meanwhile, the slope gradient was measured at the top, middle slope, and base of the slope using a digital laser level (LS160, LAISAI Laser Technology Co., CN).

In July 2023, soil samples containing ^{137}Cs were obtained by vertically inserting a soil auger with a diameter of 5 cm into the ground to a depth of 30 cm. As shown in Fig. 2, along the slope length, the distance between every two sampling points ranges from 19 to 25 m, with a total of 26 sampling points arranged on each slope. Background sampling points for ^{137}Cs were obtained from a secondary forest located within the study area, where eight background sampling points were established. The topography of this site is characterized by a flat landscape. Survey data reveal that this secondary forest has experienced minimal human disturbance since the 1960s, preserving its natural condition with negligible erosion and sediment deposition processes. Consequently, this location was designated as the ^{137}Cs background sampling site, and the measured background concentration of ^{137}Cs was determined to be 2379 Bq m^{-2}. The soil samples obtained from the experimental site were subjected to air-drying under ambient conditions. Following sun-drying, extraneous materials including stones, plant roots, and weeds were eliminated by sieving through a 2 mm sieve. The prepared samples were subsequently stored in the laboratory for subsequent analysis. Approximately 300 g of the processed sample were then accurately weighed by using a balance with a precision of 0.001 g, and subsequently transferred to a clean plastic container of comparable size. The sample should be uniformly distributed within the container through shaking, which will facilitate the attainment of a nearly level surface of the soil sample. The analytical procedure employs an ORTEC-manufactured (GMX-50220, AMETEK, USA) 8192-channel low-background γ-ray spectrometer to quantify the complete peak area of ^{137}Cs at 661.6 keV. The duration for data collection is set at 43200 s, and

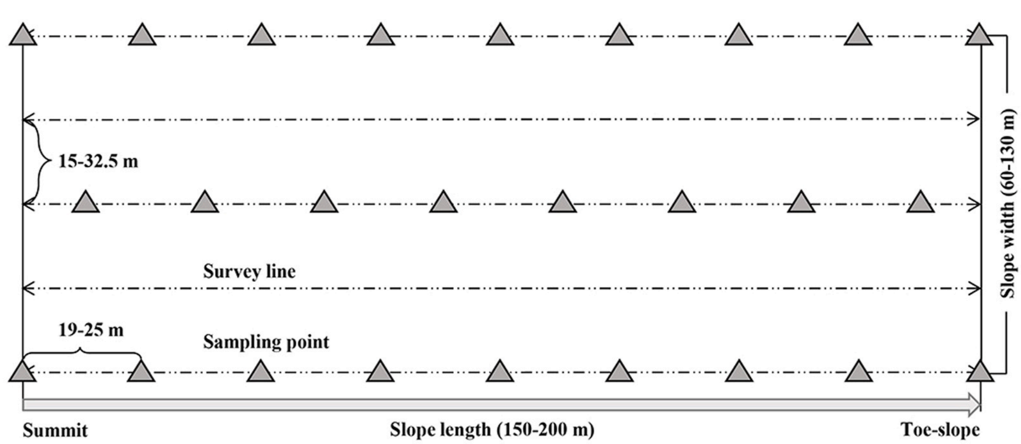

Fig. 2. Schematic diagram illustrating the arrangement of sample points on a slope.

the evaluation of the instrument's repeatability assessment indicates an error of ≤ 5 % at a 95 % confidence interval.

2.3. Determination of soil thickness using GPR

In October 2023, the BST on the slope was assessed using GPR (SIR-4000, GSSI, USA), coinciding with the period of soil property sampling. On each slope, 5 GPR (SIR-4000, GSSI, USA) survey lines were deployed, and detection was conducted using a 400 MHz antenna with the detection direction from the top to the toe. The spacings between every two survey lines were 15–32.5 m (Fig. 2). Five GPR survey lines were systematically allocated across each slope in proportion to its width. And detection was conducted using a 400 MHz antenna with the detection direction from the top to the toe. The spacings between every two survey lines were 15–32.5 m (Fig. 2). Concurrently, soil profiles were excavated at three slope positions (slope top, middle slope, and slope toe) to document the precise BST. Furthermore, markers composed of steel pipes were installed at the boundary between the black soil and the loess parent material. These steel pipes, measuring 5 cm in diameter and 60 cm in length, were embedded perpendicular to the GPR survey lines. Due to the significant difference in dielectric properties between steel pipes and the soil, distinct jump phenomena in the radar images, which are distinguishable from the signal characteristics associated with soil layers. The detection accuracy of GPR can be quantitatively assessed by comparing the depth measurements of markers observed in the radar images with their true burial depths.

The radar images obtained were processed utilizing RADAN7 software (GSSI, USA). The processing steps included time zero correction to eliminate air wave interference, background removal to reduce horizontal noise, and gain adjustment to amplify signals from greater depths. These procedures were implemented to ensure the accuracy and clarity of the resulting depth profiles. GPR operates on the principle that electromagnetic waves are reflected upon encountering interfaces between different media. Consequently, the precision of the permittivity is of paramount importance, as it directly affects the accuracy of thickness measurements. Following the processing of the radar images as previously outlined, the two-way travel time associated with the uppermost vertex of the steel pipe was initially determined. Utilizing the measured depth at the location of the steel pipe, the propagation velocity of the electromagnetic wave at that specific point was subsequently calculated. This propagation velocity was then employed to derive the soil dielectric constant, as described by Eqs. 4 and 5. Based on the calculated soil permittivity, the appropriate permittivity was incorporated into RADAN7 to transform the time-domain profile into a depth-domain profile, thereby enabling depth calibration. Additionally, by analyzing the signal characteristics of the marker layer on each survey line, we further examined the signal variation patterns of the black soil to determine the boundary of the BST (Fig. 3).

2.4. Data processing and analysis

This study employed the quality balance model to estimate the soil erosion rate by analyzing the ^{137}Cs inventory in the soil (Zhang, 1990). The equation for the model is presented as follows:

$$E = 10^3 DB\left(1 - \left(\frac{A}{A_0}\right)\right)^{\frac{1}{t-1963}} \tag{1}$$

where E is the long-term average soil erosion rate (kg m^{-2} a^{-1}); A is the surface activity of sample ^{137}Cs (Bq m^{-2}); A_0 is the baseline value of ^{137}Cs in the year of sampling (Bq m^{-2}); D is the average plow layer depth (m), 0.2 m in this study; t is the year of sampling (years), specified as 2023 in this study; and B is the soil bulk density (kg m^{-3}).

The formula for calculating the average annual soil erosion depth h (m) is:

$$h = \frac{Ea}{B} \tag{2}$$

where a is the period from 1963 to the sampling year, which is 60 years in this study; B is the annual average soil bulk density (kg m^{-3}).

The formula for calculating the BST is:

$$H_2 = H_1 + h \tag{3}$$

where H_2 is the BST in 1963 (m); H_1 is the BST sampled in the year 2023 (m).

Based on the propagation time and depth of electromagnetic waves, the propagation velocity of electromagnetic waves in the soil is calculated using the following formula:

$$v = \frac{2h}{t} \tag{4}$$

where v is the propagation velocity of electromagnetic waves in the medium (m ns^{-1}); h is the depth of the underground target (m); and t is the two-way travel time of the electromagnetic wave reflection signal in

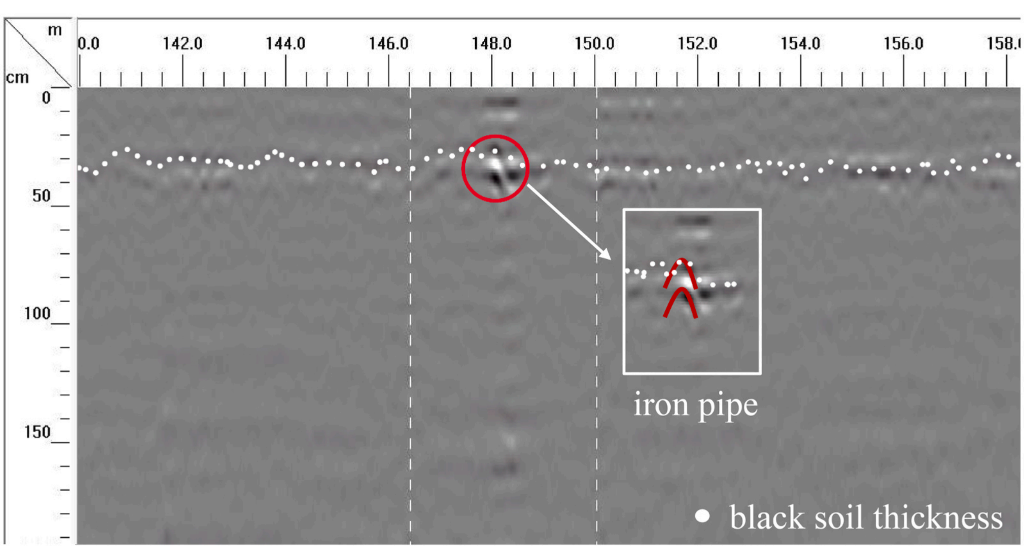

Fig. 3. Radar image of soil thickness on straight slopes. The location of the preburied iron pipe is marked with a red circle, and the boundary of black soil thickness is identified by white dots.

the medium (ns).

The permittivity can be determined based on the propagation velocity of electromagnetic waves, calculated using the following formula:

$$\varepsilon = \left(\frac{c}{v}\right)^2 \quad (5)$$

where ε is the soil permittivity; v is the propagation velocity of electromagnetic waves in the medium (m ns^{-1}); and c is the propagation velocity of electromagnetic waves in a vacuum (3×10^8 m s^{-1}).

In this study, Origin 2023 (OriginLab, USA) was employed to illustrate the contour maps of spatial distribution of soil erosion-deposition rates and BST on slopes. The soil thickness was analyzed for normal distribution and subjected to an independent samples T-test ($\alpha<0.05$) using SPSS 22.0 software. Using SPSS 22.0 software, the data were preprocessed by conducting normality tests and homogeneity of variance tests, followed by a multi-factor analysis of variance (ANOVA) on BST across different years ($\alpha<0.05$). Furthermore, a significance analysis was performed to assess the differences in BST across various years.

3. Results

3.1. Variation of soil erosion rate and BST on slopes

The soil erosion-deposition rates exhibited significant variability across various slope shapes (Fig. 4). The average soil erosion rates were ranked as follows: concave slope (2537.71 km^{-2} a^{-1}) > convex slope (2230.41 km^{-2} a^{-1}) > straight slope (1773.30 km^{-2} a^{-1}). Additionally, substantial sediment accumulation was noted at the base of both convex and concave slopes (Fig. 5). The concave slopes exhibited the greatest degree of variability in erosion rates, with a maximum variation of 78 %. For the straight slope, its erosion rate exhibits a "low-high-low" three-segment pattern with increasing slope length: in the 0–110 m slope length, the erosion rate is the lowest and concentrated in the middle of the slope (with higher values on both sides); when the slope length extends to 120–170 m, the erosion rate increases overall; while in the toe area (180–200 m), the erosion rate decreases again. The convex slope exhibited the highest average erosion rate within the slope lengths of 0–24 m and 64–96 m, reaching 2633.81 km^{-2} a^{-1}. Erosion rates progressively decreased from 100 m along the slope to its base, with localized deposition observed in lower slope sections. On slopes with lengths ranging from 15 to 45 m and 75–100 m, the average erosion rate for concave slopes was notably high at 4172.78 km^{-2} a^{-1}. However, as the slope length extended to 100 m, the erosion rate gradually decreased with an average deposition rate of 530.79 km^{-2} a^{-1}.

The fundamental principle underlying the use of GPR for detecting soil thickness is the contrast in permittivity between the target layer and the surrounding medium, which produces discernible electromagnetic wave reflections at their boundary. Although both materials are macroscopically classified as soil, our previous study (Liu et al., 2021) systematically demonstrated, through controlled laboratory and field experiments, that these materials possess markedly different physical properties. These differences lead to variations in their dielectric characteristics, thereby enabling GPR to effectively identify the interface between black soil and loess parent material. The actual buried depth and GPR measured depth of iron pipe at the top, middle, and toe of the slope, were presented in Table 2. The results indicated that GPR achieved an accuracy ranging from 87.05 % to 95.58 % in measuring BST, with no significant difference observed between the GPR measured depths and the actual burial depths.

Furthermore, our findings reveal that the BST on slopes exhibited uneven variation characteristics, a distribution pattern predominantly influenced by soil erosion and deposition mechanisms. Based on the measured data from 2023, the average BST values of the three slopes showed significant differences: convex slope (28.73 cm) > straight slope (28.09 cm) > concave slope (27.48 cm) (Fig. 5). It is noteworthy that there was an increase in the BST at the toe of all three slopes, exhibiting a relatively low degree of variability among the slopes. On straight slope at the length of 60–120 m, a notable disparity in the BST was observed,

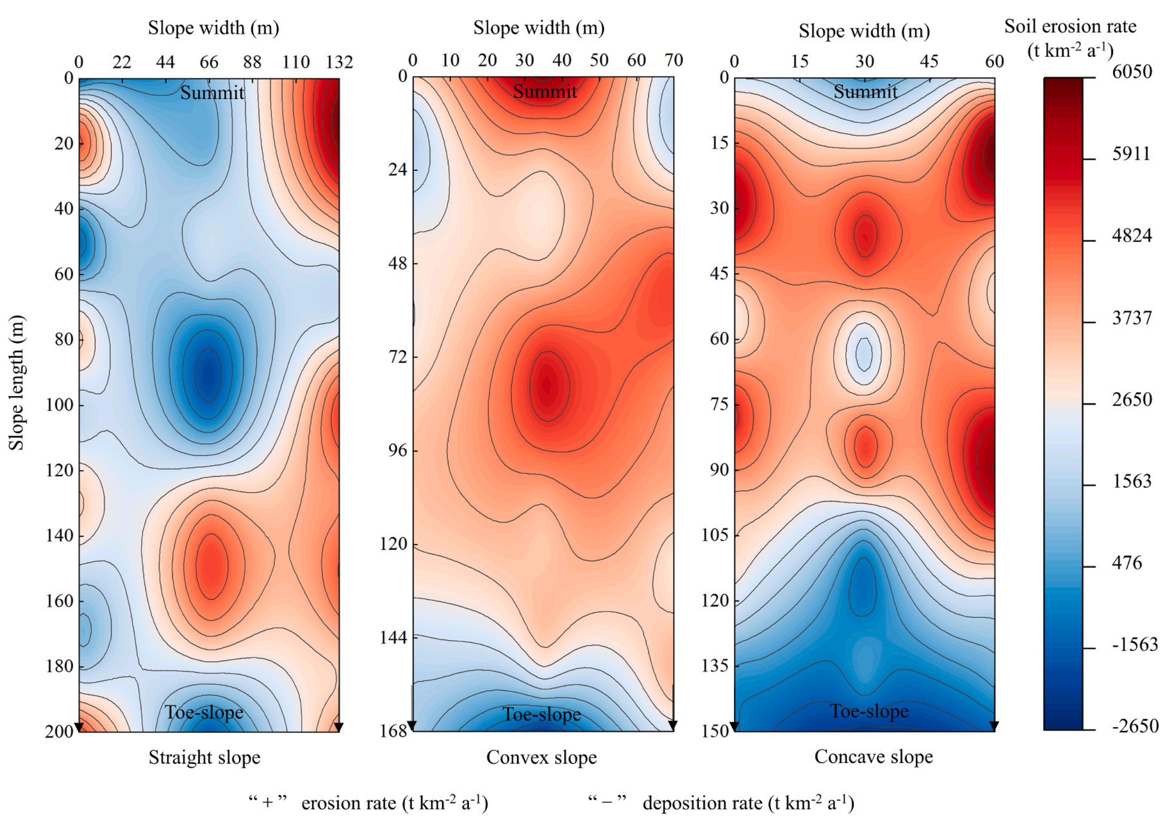

Fig. 4. Characteristics of soil erosion-deposition rate distribution on slopes with different shapes in 2023.

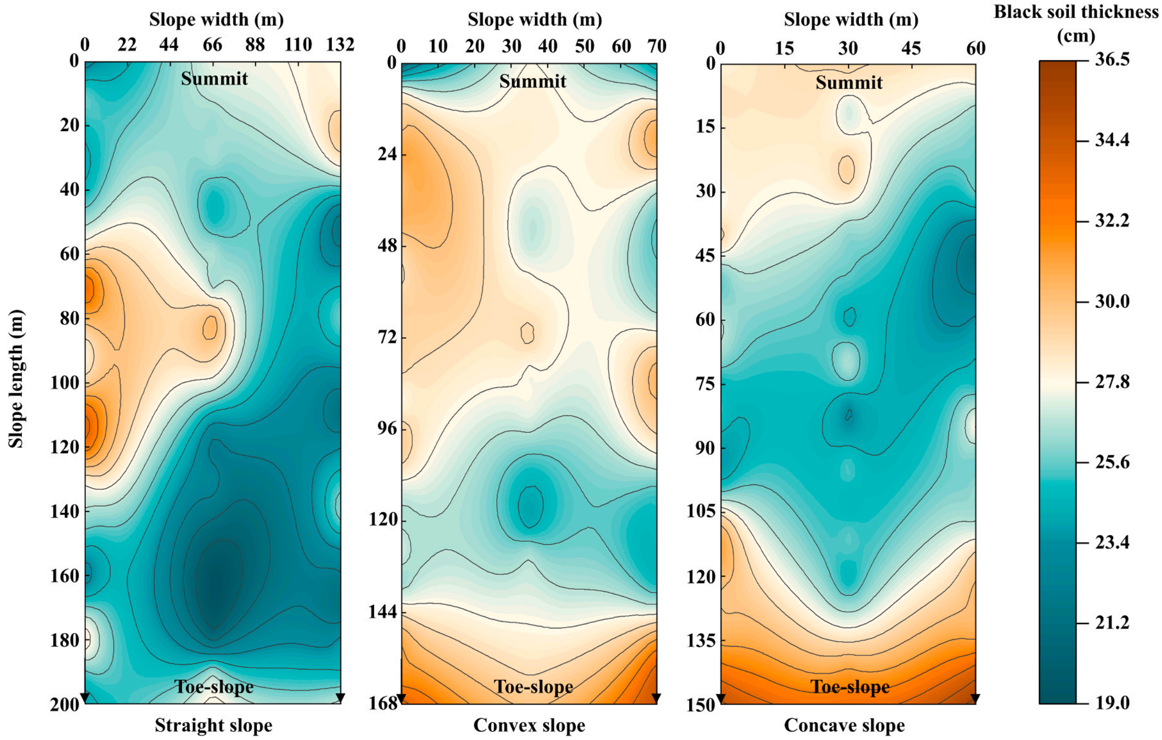

Fig. 5. Distribution characteristics of black soil thickness on slopes with different shapes in 2023.

Table 2
Actual buried depth and GPR measured depth of iron pipe with different slope shapes.

Slope shape	Actual depth (cm)	GPR measurement (cm)	Errors (%)	*P*
Straight slope	31	33.22 ± 0.29	7.16	0.744
	22.5	23.72 ± 0.95	5.42	
	20	21.68 ± 0.43	8.40	
Convex slope	19	21.46 ± 0.13	12.95	0.482
	25	26.97 ± 0.52	7.88	
	29	32.36 ± 0.57	11.59	
Concave slope	28.5	30.30 ± 0.26	6.32	0.683
	26.5	27.67 ± 0.06	4.42	
	22.5	24.01 ± 0.37	6.71	

Note: $P > 0.05$ indicates no significant difference.

with the left side exhibiting a greater depth than the right side. In the range of 150–170 m, the average BST was determined to be 25.36 cm, which subsequently increased to 28.08 cm at the foot of the slope. The BST on the convex slope changed steadily, with an average measurement of 28.98 cm observed across a slope length ranging from 24 m to 96 m. Subsequently, there was a gradual reduction in thickness, while the average thickness increased to 31.72 cm at a slope length of 144 m. Within the span of 45–90 m along the slope, a decrease in the BST was observed on the concave slope, ultimately reaching a minimum thickness of 19.18 cm. However, as the distance from the top of the slope to the toe increased, the BST exhibited a gradual increase, culminating in a thickness of 36.25 cm.

3.2. Spatial distribution of BST on slopes in 1963

Based on the 2023 BST and erosion rate data, this study reconstructed the spatial distribution characteristics of BST in 1963 (Fig. 6). The average BST of the three slopes in 1963 were significantly higher than those in 2023: concave slope (38.61 cm) > convex slope (38.51 cm) > straight slope (35.86 cm). The variation in BST on three slopes exhibited a moderate degree of variability. Overall, the BST of the straight slope in 1963 showed a decreasing trend along the slope from top to toe, but thickening occurred in local areas: the BST at the 0–40 m slope length on the right side and the 60–140 m slope length on the left side were significantly higher (with an average thickness of 40.33 cm) than those in other regions. In contrast, the thickness on the convex slope exhibited considerable variability, ranging from 18.80 cm to 54.29 cm. The average BST on the top (0–24 m) and middle sections (48–104 m) of the convex slope is measured at 40.45 cm, gradually decreasing to 35.84 cm toward the slope toe. Additionally, there is a notable variation in thickness on the concave slope, two thick zones of BST were observed at the slope top (10–45 m) and middle-lower slope (70–90 m), with an average thickness of 44.74 cm. Toward the slope toe (90–180 m), the BST gradually decreased to 33.68 cm.

3.3. The evolutionary process of black soil on slopes

Over the past semi-century (1963–2023), the average erosion rate of black soil on slopes with different shapes was 0.17 cm a^{-1}. A comparative analysis with data from 2023 reveals notable discrepancies in the reduction of thickness across different slope shapes in 1963 (Table 3): concave slopes (11.13 cm) > convex slopes (9.78 cm) > straight slopes (7.77 cm). The average erosion rate for straight slopes was determined to be 0.14 cm a^{-1}. A notable variation in thickness was observed within slope lengths of 10–30 m and 120–160 m, exhibiting reductions of 25.34 % (9.86 cm) and 26.13 % (9.54 cm), respectively (Fig. 7). At slope toe of 170–200 m, the thickness experienced a decrease of 7.51 cm, corresponding to a reduction of 21.52 %. As illustrated in Fig. 7, the decrease in the BST on straight slopes has exhibited a consistent and stable pattern, which corresponds with trends in slope gradient. This indicates that the erosion experienced over the past 60 years has not significantly modified the topographical features of these slopes.

The average erosion rate observed on the convex slope was calculated to be 0.18 cm a^{-1}. The most notable alterations in thickness were observed within the slope length of 40–104 m, with an average

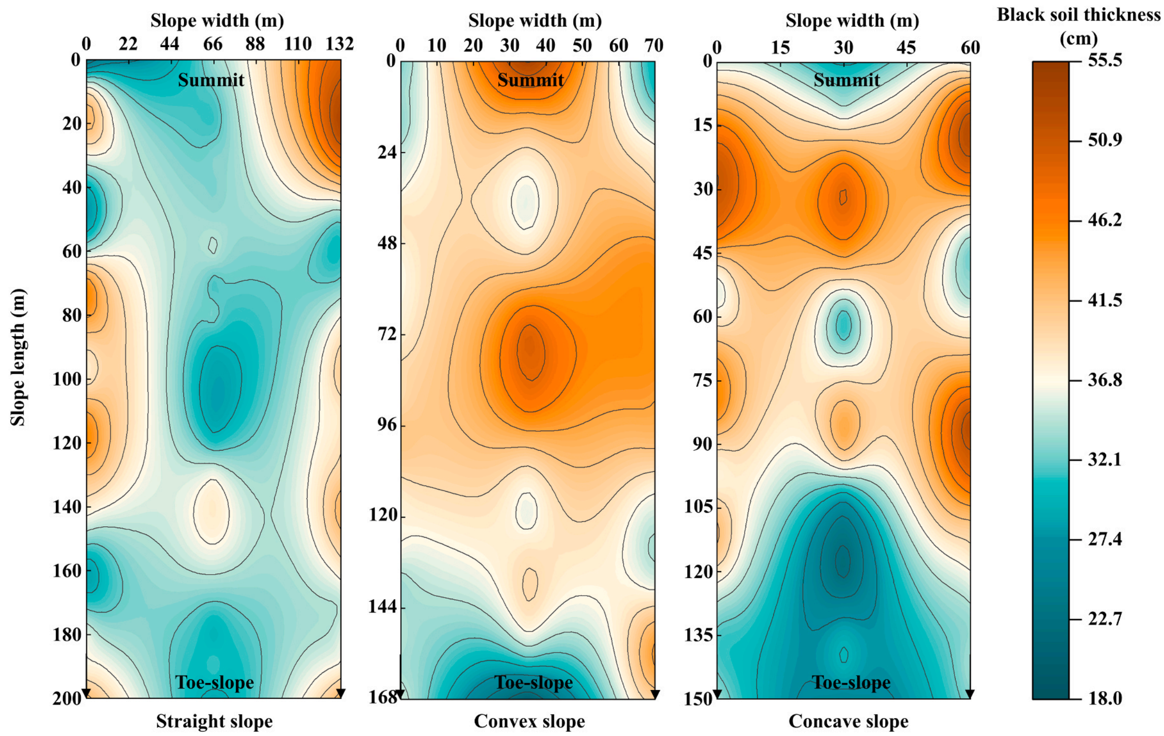

Fig. 6. Estimated distribution of black soil thickness on slopes with different shapes in 1963.

Table 3
SEDR and BST on slopes with different shapes.

Slope shapes	Parameters	Minimum	Maximum	Mean value	Standard deviation	Coefficient of variation%
Straight	SEDR (t km^{-2} a^{-1})	-54.97	3477.56	1773.30c	849.59	48
	BST (cm)	23.35	35.99	28.09 a	2.73	10
	PBST (cm)	25.17	46.52	35.86 b	4.18	12
Convex	SEDR (t km^{-2} a^{-1})	-2603.30	5816.09	2230.41b	1311.01	59
	BST (cm)	21.55	33.96	28.73 a	2.40	8
	PBST (cm)	18.80	54.29	38.51 b	5.64	15
Concave	SEDR (t km^{-2} a^{-1})	-1912.20	6017.05	2537.71a	1972.70	78
	BST (cm)	19.18	36.25	27.48 a	3.35	12
	PBST (cm)	20.34	55.29	38.61 b	7.83	20

Note: SEDR is soil erosion-deposition rate, BST is the black soil thickness in 2023, PBST is the black soil thickness in 1963. Under different slope shape conditions, different letters in the average soil thickness in 2023 (BST) and the average soil thickness in 1963 (PBST) indicate significant difference at 0.05 level. Under different slope shape conditions, different letters in the soil erosion-deposition rate indicate significant difference at 0.05 level. "+ "is erosion rate, "-" is deposition rate.

reduction of 12.71 cm was recorded, corresponding to a decrease of 30.82 %. Additionally, the average slope gradient of 3.03° also showed an increasing trend. This indicates that topographical features of this section of the slope have not been changed. At the toe of the slope, there was a notable reduction in the rate of thickness decrease. Specifically, the BST at the toe of the slope in 2023 exhibited an increase of 1.48 cm relative to 1963, corresponding to soil deposition rates of 4.74 %. Nevertheless, as the length of the slope extended to 128 m, the gradient of the slope progressively increased, ultimately attaining a peak value of 4.50°. The trend in soil erosion thickness reversed with the increase in slope length, decreasing a significant reduction up to 128 m (Fig. 8).

The average rate of thickness reduction on concave slope was 0.20 cm a^{-1}. Notably, within slope length of 10–50 m and 65–100 m, there was a significant decrease in thickness, with average reductions of 39.50 % (17.40 cm) and 39.57 % (16.63 cm), respectively. Along slopes spanning 65–100 m, the slope gradient and the erosion thickness show opposite trends, similar to the pattern observed on convex slopes. However, as the slope length reached to 110 m, the rate of thickness reduction began to decline. Specifically, within the slope length range of 140–150 m, the BST at the base of the slope in 2023 exhibited an increase of 2.33 cm when compared to 1963, resulting in a sedimentation rate of 7.53 %. This suggests that, over the past 60 years, the gradient of the slope has diminished, resulting in the deposition of some eroded black soil from the upper section of the slope at its base.

4. Discussion

4.1. Influencing factors of variations in black soil thickness

The reduction in BST is predominantly attributable to prolonged soil erosion processes. The types of soil erosion observed in black soil regions exhibit a range of diversity and complexity, marked by the interaction of multiple erosive forces and the convergence of various processes (Wang et al., 2020). The utilization of ^{137}Cs tracing technology serves as an effective approach for conducting long-term assessments of soil erosion and deposition (Wang et al., 2022). It reflects the average annual erosion rates, which directly illustrate the spatial variability of erosion rates as well as the cumulative effects of various landscape processes. These processes encompass water erosion, wind erosion, freeze-thaw cycles, and the impacts of tillage (Du and Walling, 2011). This study employed

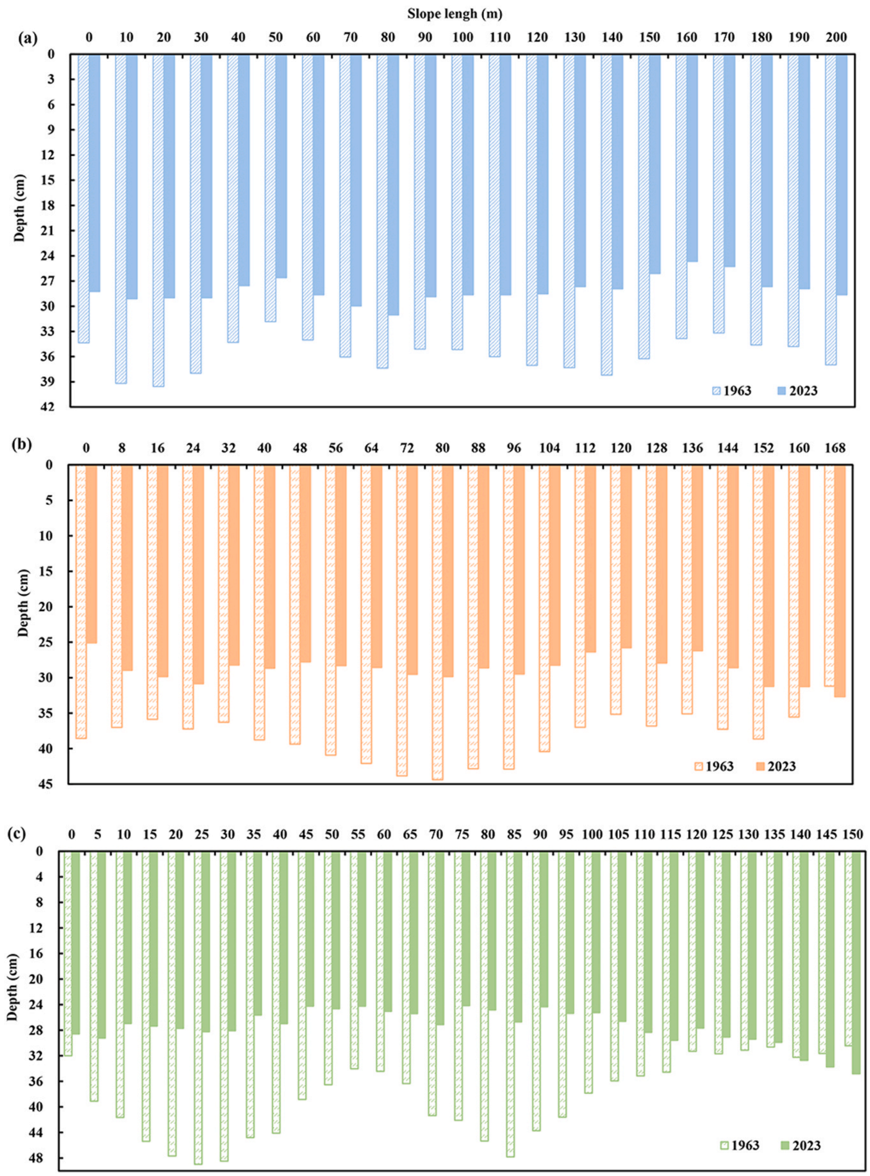

Fig. 7. Comparison of the black soil layer thickness between 1963 and 2023 on three slopes with different shapes, (a) straight; (b) convex; (c) concave.

the ^{137}Cs tracing method and revealed that erosion rates exhibit considerable spatial variability across distinct slope morphologies (Fig. 4), thereby directly influencing the spatial variation in BST. Specifically, in regions characterized by elevated erosion rates, the BST exhibits a more pronounced reduction. Conversely, in depositional zones or areas experiencing minimal erosion, the soil thickness tends to remain relatively stable or shows a slight increase. This spatial pattern suggests that the variability in BST primarily arises from the prolonged accumulation of spatial disparities in erosion rates (Liu et al., 2021).

The distinctive topographical features of the northeastern black soil region contribute to considerable erosion, which plays a crucial role in the depletion of the black soil (Liu et al., 2019). The erosion rate is concurrently influenced by both the slope topography and the characteristics of soil texture. From a topographic perspective, the findings of our study corroborate prior research (Bracken and Kirkby, 2005; Moreno de las Heras et al., 2010), indicating that the steepest concave slopes, characterized by a maximum gradient of 3.19°, experienced the highest rates of erosion alongside the most pronounced reduction in BST. Increased slope steepness facilitates greater runoff convergence and enhances scouring potential, thereby directly contributing to elevated soil loss. In contrast, the straight slope, with a minimum gradient of 1.91°, exhibited the lowest levels of erosion and the least diminution in BST. Regarding soil texture, concave slopes exhibit a greater proportion of sand compared to straight slopes. Elevated sand content frequently reduces soil aggregate stability and infiltration capacity (Wei et al., 2015), which in turn enhances surface runoff and particle transport, thereby exacerbating erosion and the reduction of BST. The interaction between slope gradient and soil texture indicates that black soil thickness evolution is shaped by the synergistic effects of multiple factors (Xing et al., 2023; Xie et al., 2023).

Erosion processes also continuously reshape slope microtopography, thereby influencing the spatial variability of BST through feedback mechanisms. Our observations indicated that throughout the erosion process occurring between 1963 and 2023, the crests of convex slopes and the depressions of concave slopes exhibited downslope migration. During the erosion process, sediment on the slope undergoes transfer. Under the combined actions of runoff detachment, scouring, and transportation, soil particles are gradually moved from the top to the toe slope, thereby progressively altering the spatial distribution of microtopography (Sun et al., 2021). Initial microtopography influences the runoff and sediment yield processes on the slope surface. Meanwhile, the development of runoff and erosion also alters the microtopographic

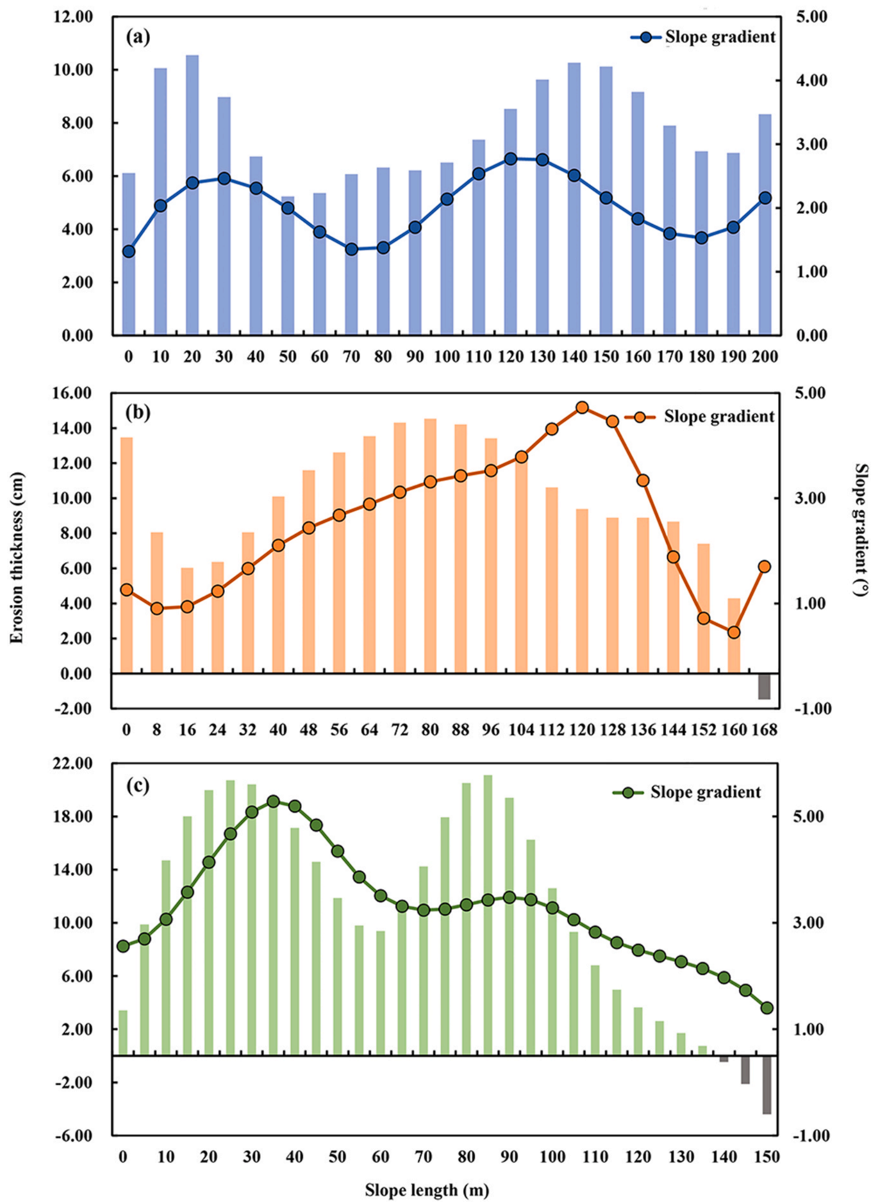

Fig. 8. Changes of slope gradient and eroded black soil layer thickness from 1963 to 2023 on three slopes with different shapes, (a) straight; (b) convex; (c) concave.

structure of the slope. This ongoing dynamic process continues to evolve as erosion persists (Zhang et al., 2022). Although the general morphology of the slope has not undergone substantial alterations to date, ongoing erosion may promote the progressive displacement of microtopographic features. This process could ultimately result in notable modifications to slope morphology and consequently lead to a redistribution of the BST.

In addition to topographical features and soil characteristics, vegetation cover and agricultural management practices constitute critical factors influencing erosion dynamics and the BST. Although the study area is a farmland ecosystem, the role of seasonal crop cover in safeguarding the soil remains significant and should not be overlooked. During the rainy season, dense crop canopies, such as those of maize and soybeans, effectively intercept rainfall and diminish the splash energy of raindrops impacting the soil surface. Concurrently, extensive root systems contribute to soil stabilization and improve its resistance to erosion (Lin et al., 2019). Within the study area, the soil remains completely bare after the autumn harvest due to the lack of vegetative residues being returned to the soil. This absence of organic inputs impedes the accumulation of soil organic matter (Blanco-Canqui and Lal, 2009). Spatially, upper slope locations are subject to increased erosion, which causes the removal of surface soil rich in organic matter, thereby reducing soil organic matter content (Ampontuah et al., 2006). In contrast, lower slope positions or depositional zones tend to accumulate soil organic matter transported from upslope areas (Berhe et al., 2012). The interval between post-harvest and the subsequent pre-sowing phase, characterized by exposed soil devoid of vegetative cover, renders the surface soil particularly vulnerable to erosion processes during the spring snowmelt period (Huang et al., 2022). Straw mulching and residue incorporation serve not only to directly shield the soil surface and reduce runoff during periods when the soil is exposed but also function as essential practices for replenishing soil organic matter and improving soil aggregation (Blanco-Canqui and Lal, 2009). Furthermore, the strategic implementation of hedgerows or terraces on sloped agricultural land effectively reduces slope length, decreases runoff velocity, and improves sediment retention. In addition, the development of regional windbreak forests serves to lower wind speeds and regulate microclimatic conditions, thereby alleviating the combined effects of wind and water erosion (Vacek et al., 2018). The lack of soil and water conservation interventions will substantially diminish the resilience of the ecosystem to erosion, consequently expediting the depletion of BST.

Moreover, regional climate variations and anthropogenic activities serve as significant factors driving alterations in the BST (Wang et al., 2013). Elevated temperatures enhance the microbial decomposition of soil organic matter (Zhang et al., 2019; Davidson and Janssens, 2006), consequently hindering the processes of black soil formation and renewal. Furthermore, prolonged continuous cropping adversely affects soil structure, enhancing its susceptibility to erosion and thereby facilitating the progressive reduction in the BST (Van Oost et al., 2009).

4.2. Trends in thickness variation of black soil

In recent years, various researchers have investigated the rate of thinning of the black soil, arriving at divergent conclusions. Fang et al. (2006) report that the northeastern black soil region experiences an average annual loss of 0.1–0.5 cm of its surface mollic horizon. Han and Zou (2021) performed an extensive examination of long-term monitoring data obtained from a fixed plot station in conjunction with ^{137}Cs computational data (An et al., 2014), utilizing a natural small watershed as the fundamental unit of analysis. The researchers conducted an analysis of soil erosion and deposition, concluding that the rate of soil loss in cultivated slopes within the northeastern black soil region ranges from 0.05 to 0.15 cm a^{-1}. Yang et al. (2011) assessed the erosion rate of the black soil in Jilin Province utilizing the RUSLE model, finding a rate of 0.035–0.2 cm a^{-1}. The depletion of the thin layer of black soil in regions characterized by thin-layered black soil (less than 30 cm) may require an estimated duration of around 200 years. In our study, the average thinning rate of the black soil in Bin County was 0.14–0.2 cm a^{-1}, a finding that aligns with the results reported by Yang et al. (2011). It is important to note that variations in study locations and methodologies may lead to discrepancies in the observed rates of black soil thinning. The majority of research employs the excavation profile method to assess the thickness of soil layers. Nonetheless, the considerable spatial variability in the distribution of BST often renders these sampling points unrepresentative, resulting in discrepancies in the survey findings. Our study employs ground-penetrating radar technology, which effectively mitigates this issue and enhances the precision of the survey outcomes.

Our study analyzes the distribution characteristics of BST over the past semi-century by integrating ground-penetrating radar technology with nuclide tracing techniques. In 1963, the BST across three slopes in Bin County varied between 19 cm and 55 cm, with an average of 37.66 cm. Simultaneously, we examined the variability in BST during this period. Despite extensive body of research on this subject, their conclusions exhibit significant discrepancies. In the 1950s, Zhu (1952) conducted an examination of the region in eastern Heilongjiang Province, focusing on areas such as Harbin, Tieli, Wudalianchi, Keshan, and Lanxi. Their study determined that the BST ranged from 40 to 80 cm. The findings from the first national soil survey indicated that before cultivation, black soil primarily exhibited a moderate thickness ranging from 30 to 60 cm, whereas instances of thicker layers exceeding 60 cm were comparatively uncommon (Zhang, 2010). We believe that the reasons for these differences include several aspects. The soil-forming conditions in the northeast China are significantly different, leading to the development of black soil horizons of varying thicknesses contingent upon these distinct soil-forming conditions (He, 1992). Furthermore, the influence of differing positions, soil sampling point densities, and measurement methods on slopes may also contribute to the observed variations in results.

In the assessment of alterations in BST over the past semi-century on the slopes, the analysis was limited to the impact of slope gradient on the BST. Subsequent investigations should incorporate other topographical variables, including slope length and aspect, to provide a more comprehensive understanding. According to our projections regarding the rate at which the black soil is being depleted, it is improbable that this layer will entirely vanish within the next 50 years. Nevertheless, without scientific and reasonable human management measures, the phenomenon of the black soil becoming increasingly thin and harder is likely to exacerbate, ultimately affecting grain production. Some studies demonstrated that the reasonable application of fertilizers (Ma et al., 2022; Ding et al., 2020) and various agricultural practices (Jia et al., 2019; Liu et al., 2012; Fang, 2021) can enhance soil fertility, reduce soil erosion, and increase crop yields to a certain degree. Furthermore, our research indicates that long-term erosion-deposition processes have the potential to modify the local topography on slopes. In the case of non-linear slopes, it is crucial to prioritize the management of steeper regions in order to mitigate the degradation of high-quality surface soil. This is crucial for the preservation of black soil, the assurance of food security, the maintenance of ecological security, and the advancement of sustainable agricultural development. These management strategies may also establish a scientific foundation for the future management of critical regions experiencing soil erosion.

This study employed GPR to estimate the BST due to its capability for continuous subsurface profiling, which offers advantages over traditional methods like soil drilling (Liu et al., 2021). However, we acknowledge several limitations that may affect the accuracy and precision of GPR measurements. Primary constraints stem from soil property variability, electromagnetic wave propagation is susceptible to fluctuations in texture, bulk density, and volumetric water content (Grote et al., 2010). Furthermore, the slope-scale approach, while detailed, cannot directly extrapolate to watershed or regional levels without additional spatial data. The reconstruction of BST changes over 60 years is based on average erosion rates, which may smooth out short-term fluctuations caused by extreme weather events or anthropogenic interventions. Future research should prioritize multi-scale sampling to improve representativeness, incorporate high-resolution remote sensing for continuous monitoring, and develop models that integrate climate factors and human activities with soil erosion dynamics.

5. Conclusions

Diverse slope configurations demonstrate distinct rates of soil erosion and deposition. Specifically, concave slopes are associated with the highest rates of erosion, whereas straight slopes demonstrate the lowest erosion rates and do not facilitate deposition. Convex and concave slopes exhibit varying degrees of sediment deposition at their bases. By comparing the BST data from 1963 and 2023, we found that in 1963, the concave slope had the thickest BST, while the straight slope had the thinnest. In 2023, the convex slope exhibited the thickest BST, whereas the concave slope showed the thinnest BST, with an overall non-uniform distribution pattern.

In the study area, the observed reduction in BST across three different slopes is recorded at 0.17 cm a^{-1}, with concave slopes declining the most. Although erosion and deposition altered local topography, the general slope forms remained unchanged. While erosion and deposition modified the local topography, the overall slope configurations remained consistent. These results contribute to the reconstruction of historical BST patterns and establish a scientific foundation for forecasting future developments, thereby providing significant theoretical and practical guidance for the conservation and sustainable management of black soil resources.

CRediT authorship contribution statement

Gang Liu: Writing – review & editing, Supervision, Methodology, Investigation, Funding acquisition, Formal analysis, Conceptualization. **Chang Liu:** Writing – original draft, Methodology, Investigation, Formal analysis, Conceptualization. **Enshuai Shen:** Investigation. **Chenxi Dan:** Investigation. **Qiong Zhang:** Investigation. **Ya Liu:** Investigation. **Chutian Zhang:** Investigation. **Han Luo:** Investigation. **Zhen Guo:** Investigation. **Kaishan Song:** Investigation.

Declaration of Competing Interest

The authors declare that they have no known competing financial interests or personal relationships that could have appeared to influence the work reported in this paper.

Acknowledgement

This research was supported by the National Key R&D Program of China (No. 2024YFD1501104), the Strategic Priority Research Program of the Chinese Academy of Sciences (No. XDA28010201), and the Natural Science Basic Research Plan in Shaanxi Province (No. 2024JC-JCQN-39).

Data availability

Data will be made available on request.

References

Ampontuah, E.O., Robinson, J.S., Nortcliff, S., 2006. Assessment of soil particle redistribution on two contrasting cultivated hillslopes. Geoderma 132 (3-4), 324–343. https://doi.org/10.1016/j.geoderma.2005.05.014.

An, J., Zheng, F.L., Wang, B., 2014. Using ^{137}Cs technique to investigate the spatial distribution of erosion and deposition regimes for a small catchment in the black soil region, Northeast China. Catena 123, 243–251. https://doi.org/10.1016/j.catena.2014.08.009.

Berhe, A.A., Harden, J.W., Torn, M.S., Kleber, M., Burton, S.D., Harte, J., 2012. Persistence of soil organic matter in eroding versus depositional landform positions. J. Geophys. Res. Biogeo 117 (G2). https://doi.org/10.1029/2011JG001790.

Blanco-Canqui, H., Lal, R., 2009. Corn stover removal for expanded uses reduces soil fertility and structural stability. Soil Sci. Soc. Am. J. 73 (2), 418–426. https://doi.org/10.2136/sssaj2008.0141.

Bracken, L.J., Kirkby, M.J., 2005. Differences in hillslope runoff and sediment transport rates within two semi-arid catchments in southeast Spain. Geomorphology 68, 183–200. https://doi.org/10.1016/j.geomorph.2004.11.013.

Davidson, E.A., Janssens, I.A., 2006. Temperature sensitivity of soil carbon decomposition and feedbacks to climate change. Nature 440 (7081), 165–173. https://doi.org/10.1038/nature04514.

Ding, J.L., Ma, M.C., Jiang, X., Liu, Y., Zhang, J.Z., Suo, L.N., Wang, L., Wei, D., Li, J., 2020. Effects of applying inorganic fertilizer and organic manure for 35 years on the structure and diversity of ammonia-oxidizing archaea communities in a Chinese Mollisols field. MicrobiologyOpen 9 (1), e00942. https://doi.org/10.1002/mbo3.942.

Du, P., Walling, D.E., 2011. Using ^{137}Cs measurements to investigate the influence of erosion and soil redistribution on soil properties. Appl. Radiat. Isot. 69 (5), 717–726. https://doi.org/10.1016/j.apradiso.2011.01.022.

Duan, X.W., Xie, Y., Ou, T.H., Liu, H.M., 2011. Effects of soil erosion on long-term soil productivity in the black soil region of northeastern China. Catena 87 (2), 268–275. https://doi.org/10.1016/J.CATENA.2011.06.012.

Emmet-Booth, J.P., Forristal, P.D., Fenton, O., Bondi, G., Holden, N.M., 2019. Visual soil evaluation - spade vs. profile methods and the information conveyed for soil management. Soil Till. Res. 187, 135–143. https://doi.org/10.1016/j.still.2018.12.002.

Fang, H.Y., 2021. Using WaTEM/SEDEM to configure catchment soil conservation measures for the black soil region, Northeastern China. Sustainability 13, 10421. https://doi.org/10.3390/su131810421.

Fang, H.Y., Sun, L.Y., Qi, D.L., Cai, Q.G., 2012. Using ^{137}Cs technique to quantify soil erosion and deposition rates in an agricultural catchment in the black soil region, Northeast China. Geomorphology 169-170, 142–150. https://doi.org/10.1016/j.geomorph.2012.04.019.

Fang, H.J., Yang, X.M., Zhang, X.P., Liang, A.Z., 2006. Using ^{137}Cs tracer technique to evaluate erosion and deposition of black soil in northeast China. Pedosphere 16, 201–209. https://doi.org/10.1016/S1002-0160(06)60044-1.

Feng, Z., Zheng, F., Hu, W., Li, G., Xu, X., 2018. Impacts of mollic epipedon thickness and overloaded sediment deposition on corn yield in the Chinese Mollisol region. Agr. Ecosyst. Environ. 257, 175–182. https://doi.org/10.1016/j.agee.2018.02.010.

Gao, X.F., Xie, Y., Liu, G., Liu, B.Y., Duan, X.W., 2015. Effects of soil erosion on soybean yield as estimated by simulating gradually eroded soil profiles. Soil Till. Res. 145, 126–134. https://doi.org/10.1016/j.still.2014.09.004.

2021. General Office of the People's Government of Heilongjiang Province, 2021. Heilongjiang Province "14th Five-Year Plan" for Black Soil Protection. https://www.hlj.gov.cn/hlj/c108373/202201/c00_31184039.shtml.

Grote, K., Anger, C., Kelly, B., Hubbard, S., Rubin, Y., 2010. Characterization of soil water content variability and soil texture using GPR groundwave techniques. J. Environ. Eng. Geophs 15 (3), 93–110. https://doi.org/10.2113/JEEG15.3.93.

Han, X.Z., Zou, W.X., 2021. Research perspectives and footprint of utilization and protection of black soil in northeast China. Acta Pedol. Sin. 58 (06), 1341–1358 (In Chinese).

He, W.Y., 1992. Heilongjiang Soils. China Agriculture press, Beijing.

Hedvall, R., Erlandsson, B., Mattsson, S., 1996. Cs-137 in fuels and ash products from biofuel power plants in Sweden. J. Environ. Radio. 31 (1), 103–117. https://doi.org/10.1016/0265-931X(95)00028-9.

Huang, D., Su, L., Zhou, L., Fan, H., 2022. Gully is the dominant sediment source of snowmelt erosion in the black soil region-A case study. Soil Till. Res. 215, 105232. https://doi.org/10.1016/j.still.2021.105232.

Jia, L., Zhao, W.W., Zhai, R.J., Liu, Y., Kang, M.M., Zhang, X., 2019. Regional differences in the soil and water conservation efficiency of conservation tillage in China. Catena 175, 18–26. https://doi.org/10.1016/j.catena.2018.12.012.

Lin, H., Xie, Y., Liu, G., Zhai, J., Li, S., 2019. Soybean and maize simulation under different degrees of soil erosion. Field Crop. Res. 230, 1–10. https://doi.org/10.1016/j.fcr.2018.10.004.

Liu, J.T., Han, X.L., Chen, X., He, R.M., Wu, P.F., 2019. Prediction of soil thicknesses in a headwater hillslope with constrained sampling data. Catena 177, 101–113. https://doi.org/10.1016/j.catena.2019.02.009.

Liu, C., Liu, G., Dan, C.X., Shen, E.S., Li, H.R., Zhang, Q., Guo, Z., Zhang, Y., 2023. Variability in mollic epipedon thickness in response to soil erosion–deposition rates along slopes in Northeast China. Soil Till. Res. 227, 105616. https://doi.org/10.1016/j.still.2022.105616.

Liu, C., Liu, G., Li, H.R., Wang, X.K., Chen, H., Dan, C.X., Shen, E.S., Shu, C.B., 2021. Using ground-penetrating radar to investigate the thickness of mollic epipedons developed from loessial parent material. Soil Till. Res. 212, 105047. https://doi.org/10.1016/j.still.2021.105047.

Liu, K., Wei, M.H., Dai, H.M., Liu, G.D., Jia, S.H., Song, Y.H., Liang, S., 2022. Spatiotemporal variation of black soil layer thickness in black region of northeast China. Geol. Resour. 31 (03), 434–442. +394. (In Chinese).

Liu, X.B., Zhang, S.L., Zhang, X.Y., Ding, G.W., Cruse, R.M., 2012. Soil erosion control practices in Northeast China: A mini-review. Soil Till. Res. 117, 44–48. https://doi.org/10.1016/j.still.2011.08.005.

Ma, P., Nan, S., Yang, X., Qin, Y., Ma, T., Li, X., Yu, Y., Bodner, G., 2022. Macroaggregation is promoted more effectively by organic than inorganic fertilizers in farmland ecosystems of China-A meta-analysis. Soil Till. Res. 221, 221. https://doi.org/10.1016/j.still.2022.105394.

Meyer, M.D., North, M.P., Gray, A.N., Zald, H.S.J., 2007. Influence of soil thickness on stand characteristics in a Sierra Nevada mixed-conifer forest. Plant Soil 294 (1-2), 113–123. https://doi.org/10.1007/s11104-007-9235-3.

Ministry of Agriculture and Rural Affairs of the People's Republic of China, 2017. Outl. Northeast Black Soil Prot. Plan (20172030). ⟨http://www.moa.gov.cn/nybgb/2017/dqq/201801/t20180103_6133926.htm⟩.

Moreno de las Heras, M., Nicolau, J.M., Merino-Martin, L., Wilcox, B.P., 2010. Plot-scale effects on runoff and erosion along a slope degradation gradient. Water Resour. Res. 46 (4), 475–478. https://doi.org/10.1029/2009WR007875.

Morey, R.M., 1974. Continuous subsurface profiling by impulse radar. Proceedings of Engineering Foundation Conference on Subsurface Exploration for Underground Excavations and Heavy Construction., New Hampshire, pp. 213–232.

Morse, M.S., Lu, N., Godt, J.W., Revil, A., Coe, J.A., 2012. Comparison of soil thickness in a zero-order basin in the oregon coast range using a soil probe and electrical resistivity tomography. J. Geotech. Geoenviron. 138, 1470–1482. https://doi.org/10.1061/(ASCE)GT.1943-5606.0000717.

National Soil Survey Office, 1998. Soils of China. China Agriculture Press, Beijing, pp. 318–336 (in Chinese).

Persico, R., 2014. Introduction to ground penetrating radar: inverse scattering and data processing. John Wiley & Sons, Inc, Hoboken.

Sorokin, A., Owens, P., Láng, V., Jiang, Z.D., Krasilnikov, P., 2020. Black soils" in the Russian soil classification system, the US soil taxonomy and the WRB: Quantitative correlation and implications for pedodiversity assessment. Catena 196, 104824. https://doi.org/10.1016/j.catena.2020.104824.

Sun, L., Guo, H., Liu, B., Wu, S., Weckler, P.R., Yang, J., 2021. Characterizing erosion processes on a convex slope based on 3D reconstruction method. Geoderma 402, 115364. https://doi.org/10.1016/j.geoderma.2021.115364.

Vacek, Z., Řeháček, D., Cukor, J., Vacek, S., Khel, T., Sharma, R.P., Kučera, J., Král, J., Papaj, V., 2018. Windbreak efficiency in agricultural landscape of the Central Europe: multiple approaches to wind erosion control. Environ. Manag. 62 (5), 942–954. https://doi.org/10.1007/s00267-018-1090-x.

Van Oost, K., Cerdan, O., Quine, T.A., 2009. Accelerated sediment fluxes by water and tillage erosion on European agricultural land. Earth Surf. Proc. Land 34 (12), 1625–1634. https://doi.org/10.1002/esp.1852.

Wang, M.Y., Shi, X.Z., Yu, D.S., Xu, S.X., Tan, M., Sun, W.X., Zhao, Y.C., 2013. Regional differences in the effect of climate and soil texture on soil organic carbon. Pedosphere 23 (006), 799–807. https://doi.org/10.1016/S1002-0160(13)60071-5.

Wang, H., Yang, S.L., Wang, Y.D., Gu, Z.Y., Xiong, S.F., Huang, X.F., Sun, M., Zhang, S., Guo, L., Cui, J., Tang, Z., Ding, Z.L., 2022. Rates and causes of black soil erosion in Northeast China. Catena 214, 106250. https://doi.org/10.1016/j.catena.2022.106250.

Wang, B.W., Zhao, X.L., Wang, X., Zhang, Z.X., Yi, L., Hu, S.G., 2020. Spatial and temporal variability of soil erosion in the black soil region of Northeast China from 2000 to 2015. Environ. Monit. Assess. 192 (6), 1–14. https://doi.org/10.1007/s10661-020-08298-y.

Wei, Y., Wu, X., Cai, C., 2015. Splash erosion of clay–sand mixtures and its relationship with soil physical properties: The effects of particle size distribution on soil structure. Catena 135, 254–262. https://doi.org/10.1016/j.catena.2015.08.003.

Xie, Y., Tang, J., Gao, Y., Gu, Z., Liu, G., Ren, X., 2023. Spatial distribution of soil erosion and its impacts on soil productivity in Songnen typical black soil region. Int. Soil Water Conse 11 (4), 649–659. https://doi.org/10.1016/j.iswcr.2023.01.002.

Xing, S., Zhang, G., Wang, C., Zhang, N., Chen, S., 2023. Effects of straw incorporation on soil erosion resistance along a land degradation gradient in the black soil region of China. Catena 231, 107365. https://doi.org/10.1016/j.catena.2023.107365.

Yang, Y.H., Yan, B.X., Zhu, H., 2011. Estimating soil erosion in Northeast China using ^{137}Cs and $^{210}Pb_{ex}$. Pedosphere 21 (6), 706–711. https://doi.org/10.1016/S1002-0160(11)60173-2.

Yang, X.M., Zhang, X.P., Deng, W., Fang, H.J., 2003. Black soil degradation by rainfall erosion in Jilin, China. Land Degrad. Dev. 14 (4), 409–420. https://doi.org/10.1002/ldr.567.

Zhang, Z.Y., 2010. The thickness changes of Ah horizon after the phaeozems cultivated. J. Heilongjiang Bayi Agric. Univ. 22 (5), 1–3 (In Chinese).

Zhang, X.B., Higgitt, D.L., Walling, D.E., 1990. A preliminary assessment of the potential for using caesium-137 to estimate rates of soil erosion in the Loess Plateau of China. Hydrol. Sci. J. 35 (3), 243–252. https://doi.org/10.1080/02626669009492427.

Zhang, X.Y., Sui, Y.Y., Zhang, X.D., Meng, K., Herbert, S.J., 2007. Spatial variability of nutrient properties in black soil of Northeast China. Pedosphere 17, 19–29. https://doi.org/10.1016/S1002-0160(07)60003-4.

Zhang, B., Zhang, M., Liu, H., Sun, P., Feng, L., Li, T., Wang, Y., 2022. Water flow characteristics controlled by slope morphology under different rainfall capacities and its implications for slope failure patterns. Water 14 (8), 1271. https://doi.org/10.3390/w14081271.

Zhang, H., Zhou, G.S., Liu, D.L., Wang, B., Xiao, D.P., He, L., 2019. Climate-associated rice yield change in the Northeast China Plain: a simulation analysis based on $CMIP_5$ multi-model ensemble projection. Sci. Total Environ. 666, 126–138. https://doi.org/10.1016/j.scitotenv.2019.01.415.

Zhu, X.M., 1952. Distribution and properties of main soils in Northeast Heilongjiang Province. Acta Pedol. Sin. 1, 1–6 (In Chinese).